

RGB Color Correction and Gamut Limitations in Smartphone-Based Kinetic Analysis of Chemical Reactions

Calum Fyfe¹, Shengkai Yu², Jing Zhang², Marc Reid^{1*}

¹*Department of Pure and Applied Chemistry, University of Strathclyde,
Royal College Building, 204 George St., Glasgow, G1 1BX, U.K..

²National Metrology Center (NMC), A*STAR, 8 Cleantech Loop,
Singapore, 637145, Singapore.

*Corresponding author(s). E-mail(s): marc.reid.100@uni.strath.ac.uk;

Contributing authors: calum.fyfe.2017@uni.strath.ac.uk;

yu_shengkai@nmc.a-star.edu.sg; zhang_jing@nmc.a-star.edu.sg;

Abstract

The variability in hardware specifications and environmental factors poses significant challenges to the use of smartphone cameras in analytical measurement. We systematically quantified multiple sources of uncertainty in smartphone-based color measurements, finding that while sensor repeatability is high ($\Delta E < 0.5$), lighting conditions and viewing angles can introduce substantial errors (ΔE increasing by up to 64% at oblique angles). We implemented and evaluated a matrix-based image color correction methodology using a color reference chart, reducing inter-device and lighting-dependent variations by 65-70% (quantified by the color change metric, ΔE). Moving beyond static image correction to video analysis, our approach was validated through the monitoring of Blue1 dye degradation kinetics using videos recorded on two different smartphones. Time-resolved and color-corrected measurements from both devices produced consistent kinetic profiles. Importantly, we identified a fundamental limitation in RGB-based colorimetry: highly saturated colors that exceed the sRGB color gamut create artificial discontinuities in kinetic profiles, manifesting as "shouldering" effects not present in spectrophotometric data. Unlike previous methods that focused on controlling environmental factors through custom enclosures, our color correction methodology systematically quantifies and corrects for multiple sources of uncertainty across various smartphone models, enabling standardized measurements even in variable conditions. This advancement enhances the reliability of field-ready, smartphone-based colorimetric applications and establishes a framework

for calibrating video-based reaction monitoring against established spectroscopic measurements.

Keywords: digital image colorimetry, video analysis, smartphone colorimetry, color correction, computer vision

1 Introduction

Digital image colorimetry (DIC) is a non-contact technique that quantifies an analyte's concentration using color values extracted from a digital image (Figure 1).

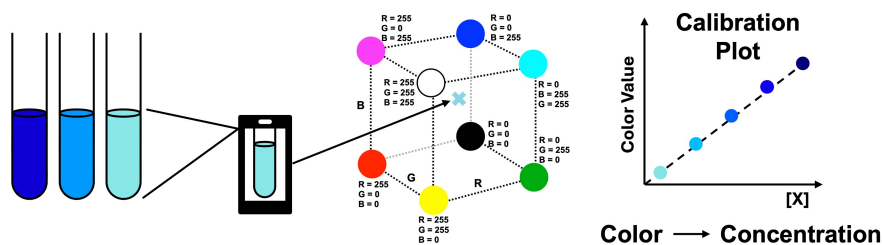


Fig. 1 Digital image colorimetry (DIC). A smartphone camera (or any device capable of capturing a digital image) is used to capture an image of the colored sample. The color values are then extracted from the image, typically expressed as RGB values. The colors from known samples are used to generate a calibration plot, which can then be used to determine the concentration of an unknown sample based on the color obtained from a smartphone image.

While applications of DIC date back to the early 2000s,[1] publication activity has since surged with the ubiquity of high-quality smartphone cameras.[2] Recent applications[3, 4] demonstrate the versatility of this approach across diverse analytical challenges: detecting disease markers in blood,[5] proline detection in food samples,[6] and ammonium and nitrate in soil samples.[7] In education, the accessibility of smartphone DIC was leveraged during the COVID-19 pandemic to enable remote practical lessons of analytical techniques.[8] There are also cases of using machine learning and artificial intelligence in DIC. [9–11] For example, Cánovas-Saura and co-workers have employed neural network-assisted procedures for visible spectrum reconstruction, using only the camera-extracted color values. Such methods have the potential to positively impact the accuracy of color measurements over large surface areas.[12]

Despite its evident applicability, DIC faces a fundamental challenge, namely the reproducibility of color values captured by different smartphone cameras used under varying conditions.[3] Unlike traditional spectrophotometers, a smartphone camera does not measure a spectrum. They capture an image by directing light through a lens system and onto an array of photosensitive sites on a semiconductor, typically covered with a Bayer color filter. A simplified overview of spectrophotometer and camera measurement methods is shown in Figure 2.

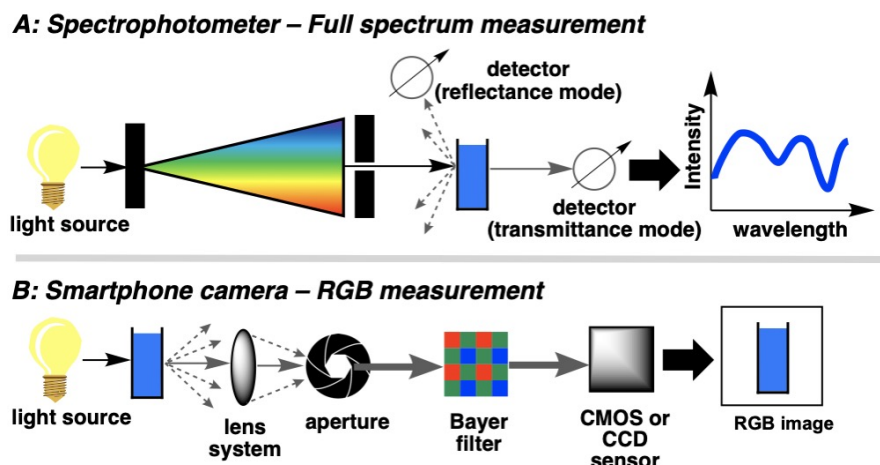


Fig. 2 Comparison of color measurement approaches. Top, A spectrophotometer measures the complete visible spectrum of transmitted or reflected light. Bottom, a smartphone camera captures color using a Bayer filter array that measures three broad color channels.

The variability of smartphone color measurement stems from two key sources: hardware diversity (e.g. phone brand + model) and capture conditions (i.e. lighting, angle, and other environmental factors). Smartphone cameras utilize different sensors, lenses, and processing algorithms that, together, affect the quantified color output.^[13] Ambient lighting conditions significantly impact color values, as smartphone cameras lack the controlled light paths of laboratory spectrophotometers.

Most current solutions to color measurement involve controlling the measurement environment through custom-designed enclosures and standardized lighting.^[14–16] A promising but underexplored approach to more robust DIC is image color correction. Image color correction is widely used in photography and digital imaging, but remains underutilized in digital analytical chemistry. Image color corrections can make DIC robust to different lighting conditions and camera sensors. Cao and Jai et al. have shown the use of image color correction to reduce external interference in smartphone DIC for paper-based colorimetric tests.^[17] Color correction was also important for machine learning training^[12].

1.1 Study Aims

Our team has developed *Kineticolor*, a computer vision software that enables video and image analysis for non-contact kinetic analysis of chemical reaction bulk. The technology has been applied, for example, to mixing analysis for reaction scale-up,^[18] high throughput kinetics and discovery,^[19] enhanced forensic spot tests,^[20, 21] and transition metal catalyst degradation.^[22] While our applications have been varied and useful, we had not, until the present study, applied any color correction methods to raw data during analysis.

This study addresses three key challenges in smartphone-based digital image colorimetry:

1. quantifying the major sources of uncertainty in smartphone color measurements, including sensor, angle, and lighting variations;
2. developing and evaluating an image color correction methodology that enables standardization across different smartphone cameras and environmental conditions; and
3. demonstrating the application of this approach to time-resolved monitoring of Blue1 dye degradation by sodium percarbonate, establishing the viability of digital video colorimetry for reaction kinetics studies.

Our results provide a practical framework for improving the reproducibility and reliability of smartphone-based video data for the purpose of time-resolved non-contact analysis of chemical and biochemical reaction bulk, as a complement to the broader suite of molecularly specific process analytics.

2 Methods

2.1 Spectra to Color

A PerkinElmer LAMBDA 1050+ UV/Vis/NIR Spectrophotometer was used to capture the visible region transmission and reflectance spectra of the samples. From the visible region, ~400 - 700 nm, transmission or reflectance spectra can be converted to color values. Formally, this involves integrating the functions of the spectral data ($R(\lambda)$) with a standard illuminant($S(\lambda)$) and standard observer functions ($\bar{x}(\lambda), \bar{y}(\lambda), \bar{z}(\lambda)$). However, as the spectral data are measured at discrete wavelengths, the computation is based on the summation of these values. The summation is shown in equation 1, which provides CIE XYZ color values. The CIE XYZ color values were calculated using the CIE D65 standard illuminant (representing average daylight with a correlated color temperature of 6504 K) and the CIE 1931 2° Standard Observer functions. These standard functions were obtained from the Commission Internationale de l'Éclairage (CIE) database at 1 nm resolution between 360 and 830 nm. The D65 illuminant was selected because it represents standard daylight conditions and is the reference illuminant for the sRGB color space.

$$X = \frac{\sum_{\lambda} R(\lambda)S(\lambda)\bar{x}(\lambda)}{\sum_{\lambda} S(\lambda)\bar{y}(\lambda)} \quad Y = \frac{\sum_{\lambda} R(\lambda)S(\lambda)\bar{y}(\lambda)}{\sum_{\lambda} S(\lambda)\bar{y}(\lambda)} \quad Z = \frac{\sum_{\lambda} R(\lambda)S(\lambda)\bar{z}(\lambda)}{\sum_{\lambda} S(\lambda)\bar{y}(\lambda)} \quad (1)$$

2.2 Color Conversions

The CIE XYZ color space is the foundational color space of the CIE system. The CIE XYZ values can be converted to other color spaces. CIE xyY is another useful color space. It is common to see this information as an xy chromaticity diagram to compare the color of samples independent of illuminance (Y).

$$x = \frac{X}{X + Y + Z} \quad y = \frac{Y}{X + Y + Z} \quad Y = Y \quad (2)$$

CIE L*a*b* is another useful color space. It is intended to be a perceptually uniform color space. It is based on the opponent model of human vision, where red and green form an opponent pair, and blue and yellow another. The relationship between the L*, a*, and b* channels to the XYZ color space are shown in equations 3 – 5. This color space is beneficial for comparing colors via the color-agnostic color difference (or contrast) metric, ΔE , the definition of which is defined later in the paper.

$$L^* = f\left(\frac{Y}{Y_n}\right) - 16, \quad (3)$$

$$a^* = 500\left(f\left(\frac{X}{X_n}\right) - f\left(\frac{Y}{Y_n}\right)\right), \quad (4)$$

$$b^* = 200\left(f\left(\frac{Y}{Y_n}\right) - f\left(\frac{Z}{Z_n}\right)\right) \quad (5)$$

where t is $\frac{X}{X_n}$, $\frac{Y}{Y_n}$, or $\frac{Z}{Z_n}$

$$f(t) = \begin{cases} \sqrt[3]{t} & \text{if } t > \frac{6}{29}^3 \\ \frac{841}{108}t + \frac{4}{29} & \text{otherwise} \end{cases}$$

For D65	For D50
$X_n = 95.0489$,	$X_n = 96.4212$,
$Y_n = 100$,	$Y_n = 100$,
$Z_n = 108.8840$	$Z_n = 82.5188$

The CIE XYZ values can also be transformed into variations of the RGB color space. The most common variant is D65 sRGB color space. CIE XYZ is converted to D65 sRGB through linear RGB D65.

$$\text{CIE XYZ to linear rgb D65} \begin{bmatrix} r \\ g \\ b \end{bmatrix} = \begin{bmatrix} 3.2405 & -1.5371 & -0.4985 \\ -0.9693 & 1.8760 & 0.041556 \\ 0.0556 & -0.2040 & 1.0572 \end{bmatrix} \begin{bmatrix} X \\ Y \\ Z \end{bmatrix} \quad (6)$$

$$\text{linear rgb D65 to D65 sRGB} \quad V = \begin{cases} 12.92v & \text{if } v \leq 0.0031308 \\ 1.055v^{\frac{1}{2.4}} - 0.055 & \text{otherwise} \end{cases} \quad (7)$$

$$v \in r, g, b$$

$$V \in R, G, B$$

2.3 Color Difference Measurements

In all cases where the contrast or difference between two color or light samples was required, the suite of ΔE definitions, derived from CIE-L*a*b* color measurements, were applied. All ΔE definitions are available in the ΔE measurement script available in the supporting information, including ΔE_{94} , ΔE_{2000} , and ΔE_{CMC} .

For a straightforward demonstration of improvement (or not) in color agreement after correction, the simplest definition, ΔE_{76} , was applied throughout this manuscript. It is defined by the Euclidean (straight line) distance between two colors across L*a*b* space.

$$\Delta E_{76} = \sqrt{(L_2^* - L_1^*)^2 + (a_2^* - a_1^*)^2 + (b_2^* - b_1^*)^2} \quad (8)$$

Where L_1^*, a_1^*, b_1^* are the CIELAB coordinates of the reference color and L_2^*, a_2^*, b_2^* are the CIELAB coordinates of the sample color. See also Figure 6.

2.4 Correction Methods

Reflectance Spectra Correction

A reflectance standard with a known reflectance, traceable to national or international standards, can be used to correct the reflectance spectra of other samples. We used Opal JK97 as a white reflectance standard (WS). Reflectance spectra, S_R , were corrected using this standard, correcting for the difference between the known reflectance of the standard WS_{known} to that measured by the instrument WS_R .

$$S_{R_{corrected}} = S_R \cdot \frac{WS_{known}}{WS_R} \quad (9)$$

Color Correction

Color correction involves transforming the RGB values of an image to match a set of reference color values measured on an independent instrument. This transformation can be represented as a linear mapping using a 3×3 correction matrix, M . Reference color values can be taken from a manufacturer or from experiment (e.g. from reflectance spectra). Commercially available color charts, such as the Datacolor Spyder Checkr 24 provides a 6×4 card of known color values: Aqua, Lavender, Evergreen, Steel Blue, Classic Light Skin, Classic Dark Skin, Primary Orange, Blueprint, Pink, Violet, Apple Green, Sunflower Primary Cyan, Primary Magenta, Primary Yellow, Primary Red, Primary Green, Primary Blue, Card White, 20 Gray, 40 Gray, 60 Gray, 80 Gray, and Card Black. The RGB values for these 24 colors can be used as reference colors for camera image color correction. With the Datacolor Spyder Checkr 24 made visible within the camera's field of view, it enables color correction

of the whole image (or series of video frames) recorded on the camera. With both the color chart references colors – $R_{ref(n)}$, $G_{ref(n)}$, and $B_{ref(n)}$ – as determined from the spectra, and the corresponding colors extracted from the image/video frame, then a 3x3 correction matrix, M , can be determined. Determining M was approached programmatically in Python using a least-squares optimization approach implemented in NumPy (numpy.linalg.lstsq). This method minimizes the sum of squared differences between the reference colors and the measured colors, determining M to minimize the difference between the reference color values and those captured in the image or video frame (equation 10). Once M has been determined, it can be applied to all pixels in an image to correct the color in the whole image or video frame.

$$\begin{bmatrix} R_{ref1} & G_{ref1} & B_{ref1} \\ R_{ref2} & G_{ref2} & B_{ref2} \\ \vdots & \vdots & \vdots \end{bmatrix} = M \times \begin{bmatrix} R_1 & G_1 & B_1 \\ R_2 & G_2 & B_2 \\ \vdots & \vdots & \vdots \end{bmatrix} \quad (10)$$

2.5 Reaction Monitoring Experiments

Blue1 Dye Stock Solution

A 10 mM stock solution of Blue1 (1 mmol, 0.792 g) was prepared in a 100 mL volumetric flask. The 10 mM stock was used to prepare all the Blue1 calibration samples and Blue1 samples for the degradation experiment.

Calibration Samples

Calibration samples (3 mL each) were prepared in standard 1 cm path length cuvettes from the 10 mM stock solution of Blue1 through a series of dilutions, producing calibration solutions of 5, 3, 1, 0.5, 0.1, 0.05, 0.03, 0.01, 0.005, 0.003, 0.001, 0.0005, 0.0003, and 0.0001 mM.

Degradation Experiments

0.3 mL of the 10 mM stock solution of Blue1 and 2.6 mL of water were added to a cuvette (path length = 1 cm). Next, 3 mL of a 0.3 M sodium percarbonate (0.141 g) working solution was prepared. The sodium percarbonate solution was only prepared as and when needed as the percarbonate solution decomposes in aqueous solution. Once prepared, 0.1 mL of the sodium percarbonate working solution was transferred to the cuvette containing Blue1, using a micropipette to begin the dye degradation experiment. The resultant solution was mixed by repeatedly dispensing and withdrawing the solution with the micropipette. After mixing, the reaction progress was followed either by a spectrophotometer or by a video captured using one of two smartphone models employed in this study.

2.6 Imaging Methods

Two smartphone cameras were used to capture images and video:

1. **iPhone 14 Pro** (48 MP, f/1.8 aperture, 24 mm equivalent focal length main camera, sensor sony IMX803 quad-Bayer CMOS sensor). The 3rd party camera app Halide Mark II Pro was used to enable more control over the camera settings when capturing images. Videos were captured using the native iOS Camera app.

2. **Samsung S23** (50 MP, f/1.8 aperture, 23 mm equivalent focal length, main camera, Samsung ISOCELL GN5 CMOS sensor). The 3rd party Open Camera app was used for the capture of both images and videos.

An indicator transfer stand and bike smartphone holder were used to secure the smartphone during image or video capture, ensuring a steady, unmoving field of view was recorded in the images and video frames. The level functionality in the iPhone's native Measure app was used to control the capture angle. In relation, the distance between the camera lens and the sample was maintained.

2.7 Code

To support core spreadsheet-based analysis, a collection of Python scripts were developed to enable and automate spectral and image/video data processing. The main analytical workflow is illustrated in Figure 3. The Python scripts, documentation, and example inputs (where appropriate) are all provided in the supporting information.

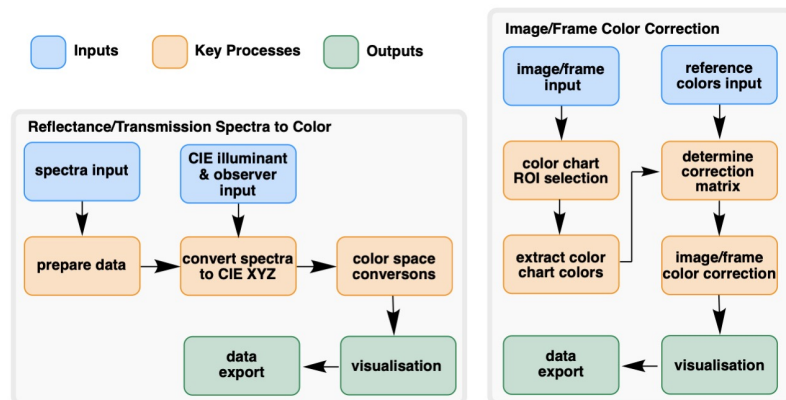


Fig. 3 Overview of the analytical workflow developed for color correction and calibration in video-based reaction monitoring. The diagram illustrates the relationship between key steps for image extraction, region of interest (ROI) selection, color calibration, and time-resolved analysis. The workflow enables standardization of color monitoring measurements across different cameras and lighting conditions.

Spectra to Color

Wavelengths and intensity responses were extracted from the spectrophotometer output .acs file, removing unnecessary data for the color calculation. With the transmittance or reflectance data provided, the Python script used to handle the spectrum to color conversion can also handle corrections to white and black reflectance standards. With the spectral data, corrected or not, the CIE Standard illuminants and

observer functions are filtered based on the sample wavelengths measured. The XYZ values were then calculated and translated into other color spaces, such as CIE xyY, CIE L*a*b*, and sRGB.

Image Analysis and Comparison

Image analysis involved loading an image and selecting a region of interest (ROI). RGB summary statistics (mean, mode, median, etc.) were determined from all the pixels included in the ROI. The mean RGB color values were then used for conversion to the other color spaces. Two images can be loaded for comparison, and the user can select an ROI on each image. The script then calculates the average RGB values of the pixels in each ROI and converts them to CIE L*a*b* to enable color difference between the ROIs to be calculated via ΔE .

Image Color Correction

Reference color values are preloaded in the program from a JSON file containing the spectra-determined color values of a Datacolor Spyder Checkr 24. First, the image to be color-corrected is loaded. The script then enables the user to position a 6 x 4 grid over the Datacolor Spyder Checkr 24 in the image. Once positioned, the image is ready for correction. The average RGB color value is extracted from the pixels from each grid square. Now, with the reference values of the squares and those from the images, the 3x3 correction matrix is determined using the NumPy linalg.lstsq method, a least squares approach for matrices. This method returns the matrix that, when multiplied with the image square color values, returns values that match the reference colors or at least a closer match. With M determined, the image can be color-corrected by applying M to all pixels. For comparison, the script calculates ΔE of the color chart colors before and after correction compared to the reference value. A batch version was developed to take a folder of images as an input, intended for color correction of extracted video frames, where the color chart does not move such that the same grid positioning works for all images.

Video Analysis

The first step was to load a video and extract the frames based on a user-defined frame sampling rate. Each frame was cropped to a user-selected region of interest (ROI). One ROI was set and applied to cropping of all subsequent frames. The extracted frames were saved individually with names based on the time each frame appeared in the video. Batch image color correction was applied to the folder of extracted frames. Like the image analysis, the average color values were determined from within the ROI of each extracted video frame in the folder, producing time series data based on averaged color.

3 Results

3.1 Characterization of Reference Color Standards

Our study began with color measurements of tiles on a Datacolor Spyder Checkr 24. This color palette was used as a set of reference colors for comparison to smartphone color measurements and to enable color correction referenced against spectral measurements. The color patches that span a wide gamut, providing comprehensive coverage of the color space. The non-glossy surface of each color patch minimized specular reflections that could otherwise have interfered with color measurements, particularly at different angles. The reference colors were determined from the reflectance spectrum of the 24 colored squares. Figure 4 shows an example of one color from the color chart. All 24 reflectance-determined colors are shown on a CIE xy chromaticity diagram to visualize the chromaticity distribution.

3.2 Quantification of Uncertainty Sources in Smartphone Colorimetry

To develop an effective color correction strategy for video-based reaction monitoring, we first quantified the major sources of uncertainty in smartphone color measurements. To evaluate the magnitude of the impact of the various sources of uncertainty in color, CIE 1976 ΔE was used to quantify the color difference (equation 8 above, and Figure 5 below). We systematically evaluated three primary factors: sensor hardware variability (i.e. different smartphone models), capture angle, and illumination conditions.

Lighting

We investigated the impact of lighting on color measurement using several different light sources. The CIE D-series is a set of spectral power distributions of daylight representing the average sunlight common conditions – D65 approximating noon daylight and D50 approximating horizon light. However, producing the exact D-series spectrum experimentally can be challenging. There are commercially available lights that report close spectral matches and, therefore, high color rendering properties. As a practical example, we had access to the YujiLEDS Normlite, an ISO3664:2000-compliant D50 light source. Under this light source, the color chart was captured with both smartphones, and the colors were compared to the colors measured by reflectance under D50 light using ΔE_{76} (hereafter referred to simply as ΔE). Using ΔE to quantify the difference in the colors under different lighting (i.e. D50 vs D65) and captured using different smartphones (i.e. iPhone vs Samsung), the summarised results are shown in Figure 5.

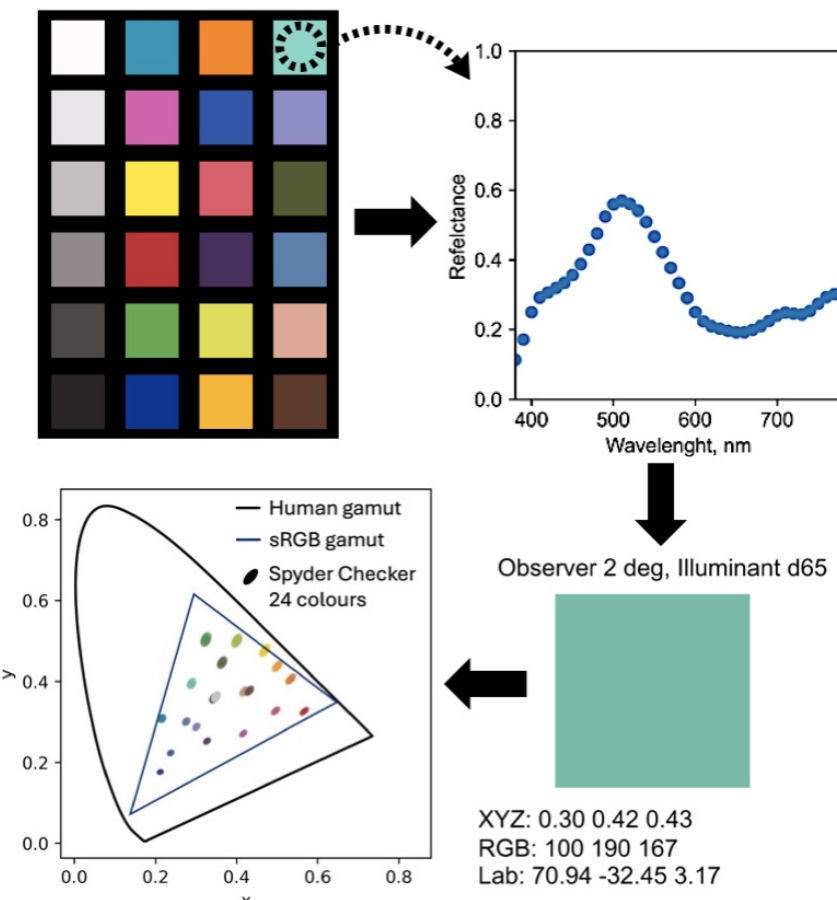


Fig. 4 Characterization of reference color standards. Top left: The Datacolor Spyder Checkr 24 color chart used for color correction. Top right: Measured reflectance spectrum for the Aqua color patch (top right patch on the color card). Bottom right: color values calculated from the spectrum. Bottom left: Distribution of all 24 reference colors on the CIE xy chromaticity diagram, illustrating their coverage within the sRGB color gamut (represented by the triangle).

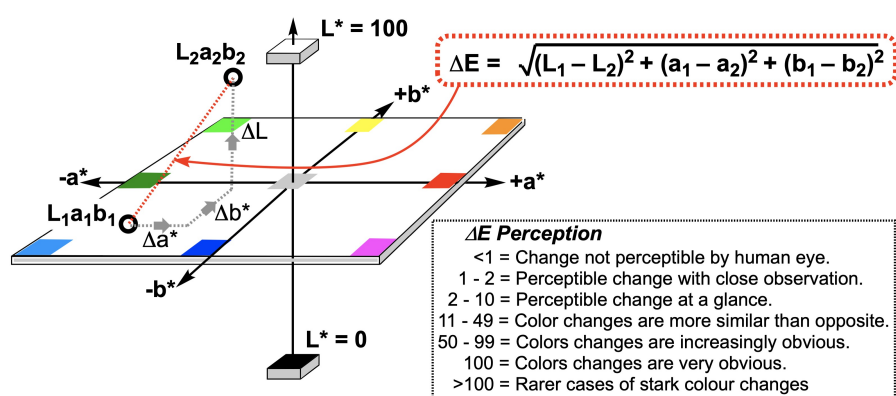


Fig. 5 A representation of ΔE and its simplest mathematical definition.

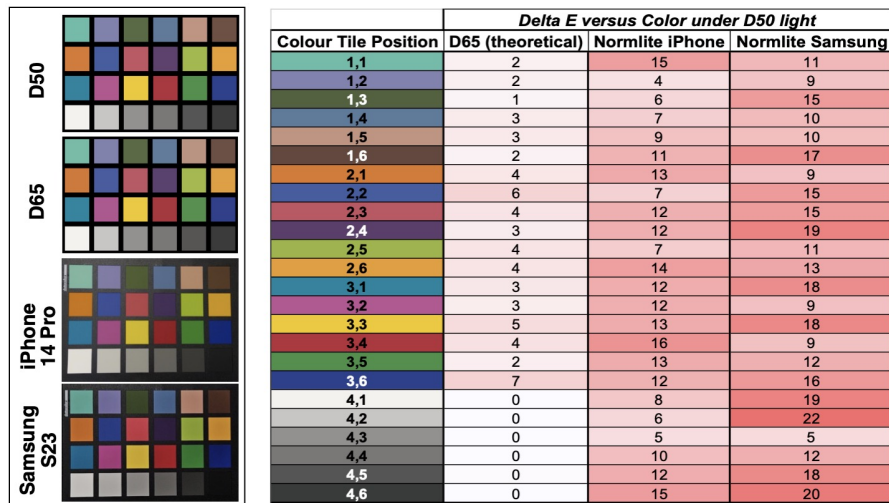
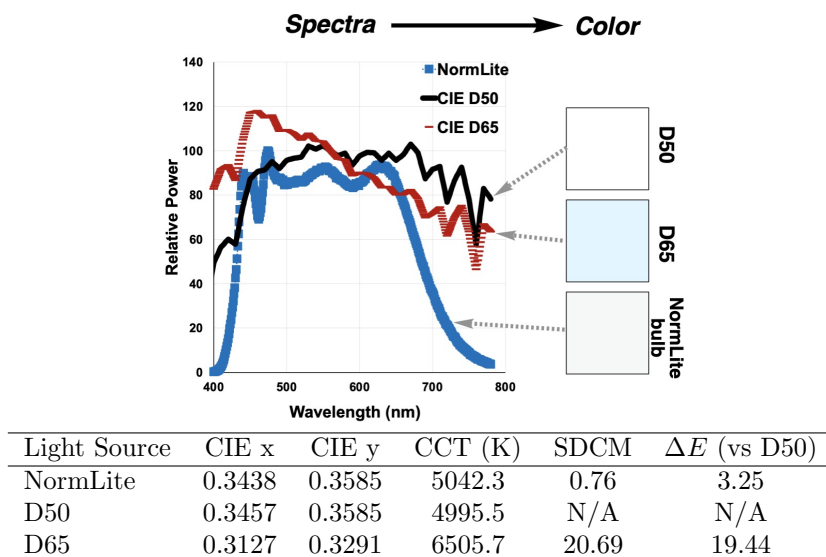


Fig. 6 Left: Pictures representing the 24-color tile under different photographic conditions. Right: Summarised ΔE values when comparing the theoretical D50 to D65 and smartphones (auto-white balance, f/1.8, manual exposure 1/60) under the Normlite D50 bulb.

The color difference between smartphone measurements under the Normlite illuminant and reflectance spectral measurements under D50 was found to be significantly greater than expected. This discrepancy far exceeded the theoretical color difference that should exist when viewing the color patches under two different standard illuminants (D50 versus D65). Moreover, there are differences between the smartphones with regards to how much each smartphone color measurement deviated from the D50 reflectance color measurements. The median ΔE versus spectral measurement was 11.8 for the iPhone and 14.2 for the Samsung. Several factors contribute to the observed differences between the phones. First, the Normlite bulb does not perfectly match the D50 standard illuminant. To characterize this discrepancy, we measured the Normlite bulb's emission spectrum and investigated its color values and metrics, as summarized in Table 1.[23, 24]

Given the difference in the bulk color properties determined from the spectra, camera settings significantly contribute to observed (i.e. detected) color distribution. The color properties suggest that the colors from the Normlite should be closer to the D50 illuminant than to the D65 variant.

Table 1 Relative power spectra for CIE D50, CIE D65, and Normlite. From the spectra, color properties were calculated and tabulated for comparison. CIE x, CIE y: Chromaticity coordinates in the CIE 1931 color space that specify the color appearance independent of brightness. CCT: Correlated Color Temperature, measured in Kelvin, represents the temperature of an ideal black body radiator whose perceived color most closely resembles that of the light source. Lower values (2700-3000K) appear warm/yellow, while higher values (5000-6500K) appear cool/blue. SDCM: Standard Deviation of Color Matching, a measure of color consistency or deviation. One SDCM step is approximately the smallest color difference the human eye can detect. Lower values indicate better color consistency and closer match to a reference.



Camera Settings

Standard camera settings such as shutter speed and ISO sensitivity change the amount of light that reaches the sensor and the sensor's response to incoming light, respectively. Settings at the extremes produce images that are under (too dark) or over-exposed (too light, washed out). Smartphones typically automate settings based on environmental lighting, but the exact settings can be variable for a given capture environment. To demonstrate these effects, we captured some qualitative examples, as shown in Figure 7.

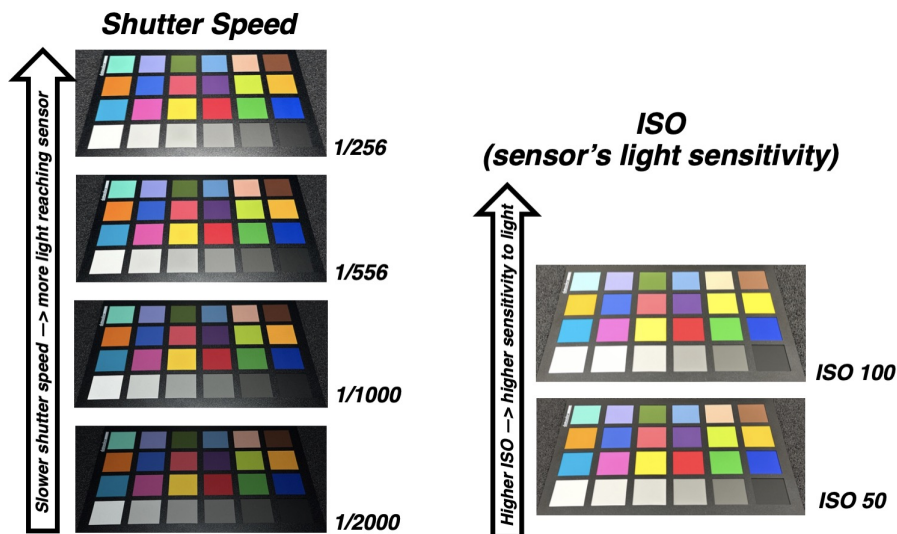


Fig. 7 Qualitative demonstration of how observable colors in an image depend on camera settings. Left: The more slowly the camera's shutter closes, the more light is captured by the sensor before the image is fully captured. Right: The higher the ISO number, the more sensitive the camera's sensor is to light, resulting in a brighter image.

Repeatability between identical measurements

Sensor repeatability was tested. The results are shown in Figure 8. The sensor repeatability for the smartphones tested is similar; the mean ΔE values are 0.46 and 0.44, and standard deviations are 0.27 and 0.23. These values are below human perception but detectable to the camera.

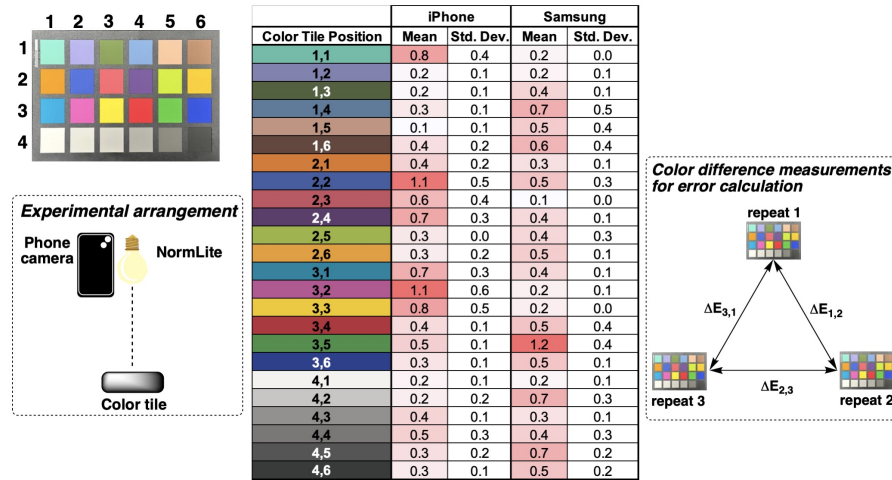


Fig. 8 Quantification of smartphone camera uncertainty between repeated image measurements. Sensor variability shown as the mean ΔE and standard deviation across three repeated captures of each color patch using iPhone 14 Pro and Samsung S23 under identical conditions (auto white balance, f/1.8, exposure 1/50). The mean ΔE color differences in the table are calculated from averaging the three three ΔE comparisons between the three repeat measurements ($\Delta E_{3,1}$, $\Delta E_{2,3}$, and $\Delta E_{1,2}$). Overall, the data show that there is very low error between repeat measurements for images captured and analyzed under the same conditions, regardless of which phone camera was used.

Image capture angle

Beyond camera settings, the capture angle can also impact the recorded color. Interactions between incident light and the material whose color is being measured can impact the light reaching the sensor, impacting both the transmission intensity and wavelength distribution. When light interacts with a surface, the reflected intensity follows Lambert's cosine law, which states that the observed intensity is proportional to the cosine of the angle between the surface normal and the direction of observation. Consequently, as the viewing angle becomes more oblique (shallower), the apparent intensity of light reflected from an overhead source diminishes proportionally to $\cos(\theta)$, where θ is the angle from the normal. Additionally, thin-film interference can cause constructive and destructive interference at different angles for different wavelengths due to refraction differences at a material surface layer, which is common in coatings.

To investigate angle effects, the color chart was captured from three angles: 15°, 45°, and 75°. Our analysis of angular effects on smartphone color measurements revealed a systematic increase in color distortion as the viewing angle became more oblique. Figure 9 presents the ΔE values between reference reflectance measurements and smartphone-captured colors at the three specified viewing angles (15°, 45°, and 75° from normal).

The mean ΔE values increase progressively from 11 at near-normal incidence (15°) to 14 at intermediate angles (45°), reaching 18 at highly oblique angles (75°). This represents a 64% increase in color distortion across the tested angular range. Particularly notable is the pronounced angular sensitivity of specific colors. Blue-toned patches (positions 2,2 and 3,6) exhibited the most dramatic angular dependence, with

ΔE values increasing by 240% and 229% respectively between 15° and 75° angles. Conversely, several patches (1,3; 2,1; 4,5) showed minimal angular sensitivity or even decreased ΔE values at more oblique angles.

These findings highlight that angular positioning is a critical consideration in smartphone colorimetry applications, particularly for blue-dominant samples. The observed color-specific angular dependencies suggest that accurate color reproduction requires either strict control of viewing geometry or appropriate angular correction algorithms, especially when working with samples containing highly saturated blue components.

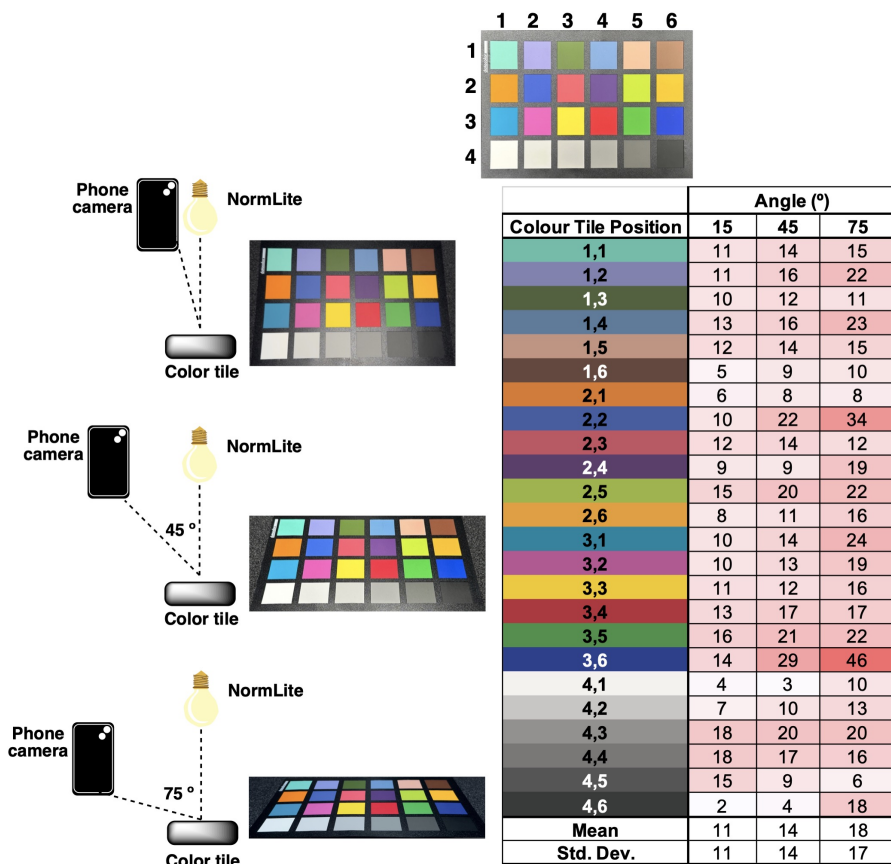


Fig. 9 Angular dependence of color measurement, showing ΔE values for color patches captured at three different angles (15°, 45°, and 75° from normal), with the measurement setup illustrated. For this demonstration, all measurements were carried out using the iPhone 14 Pro.

3.3 Effectiveness of Image Color Correction

Image correction proves effective for unifying colors captured by different cameras under varying environmental conditions. Our implementation employs a linear transformation matrix, which offers computational efficiency and is widely adopted in digital imaging applications. However, this simplified approach may not fully account for the complex, non-linear relationships between camera sensors and ambient lighting conditions. Alternative methods, such as non-linear correction models, can provide improved accuracy by accounting for inherent non-linear characteristics in color reproduction. These sophisticated approaches, however, require careful tuning to avoid overfitting, particularly when applied across different devices or environments, and typically demand greater computational resources.

The choice of color space significantly impacts correction performance. While sRGB is the native format for most smartphone images, it remains device-dependent. Performing color correction in the CIE L*a*b* color space, a device-independent system, may enhance correction quality since it is designed to be perceptually uniform and effectively decouples brightness from chromaticity. Nevertheless, converting to L*a*b* introduces additional complexity, as the accuracy of such corrections relies on consistent white point assumptions and proper linearization of RGB data. These processing steps can be error-prone, particularly with smartphone images that have undergone proprietary in-camera processing.

Figure 10 demonstrates how the color correction technique we applied substantially unifies color reproduction across different the cameras under varied lighting environments. The color chart images captured under the NormLite bulb (approximating D50 illuminant) show marked improvement after application of the correction algorithm. Quantitatively, the effectiveness of color correction is evident through the substantial reduction in ΔE values across the color gamut. Before correction, the mean ΔE across all color tiles was 16.4, indicating significant deviation from reference values derived from reflectance spectra. After correction, this mean value decreased to 8.0, representing an average improvement of 51%.

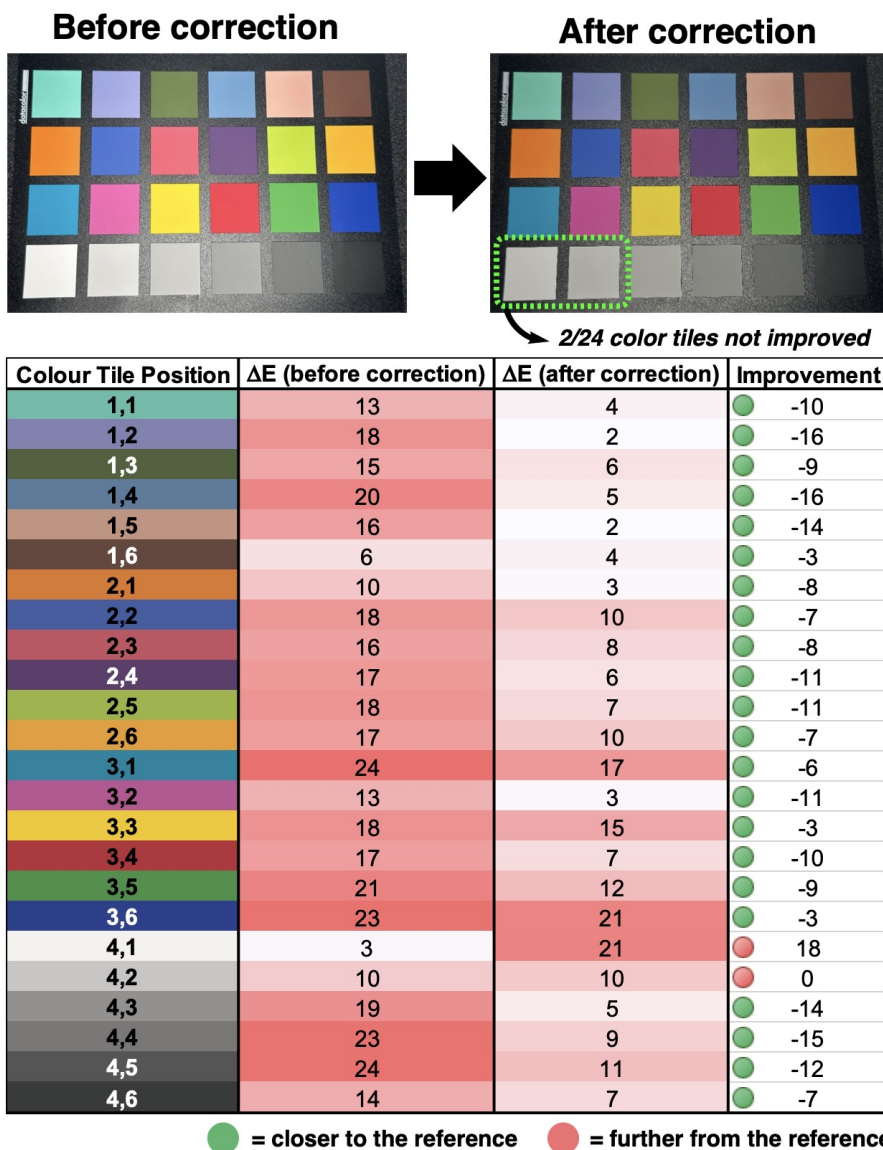


Fig. 10 Top: Color chart images are captured under the NormLite bulb (~D50), before and after color correction. Bottom: ΔE values for each color pre- and post-color correction, referenced against the color of each tile taken from the reflectance spectra. Images captured on iPhone 14 Pro, using auto white balance and exposure. In 22 of 24 color tiles, color correction brought the tile color closer to the reference, with the two tiles closest to white being the only tiles for which color correction took the color further from the reference. Additional examples under two other light sources are available in the supporting information.

The correction was particularly effective for chromatic tiles, with the most dramatic improvements observed in lavender (position 1,2; 89% reduction in ΔE), steel blue (position 1,4; 75% reduction), and classic light skin (position 1,5; 88% reduction). Notably, 22 of the 24 color tiles (92%) showed improved color accuracy after correction. The only exceptions were the two tiles closest to white (positions 4,1 and 4,2), with one showing increased deviation and one remaining unchanged. This pattern suggests a limitation in the linear correction model when handling near-white colors, potentially due to sensor saturation effects or white balance algorithm interference.

The results demonstrate that our color correction methodology significantly enhances the accuracy of smartphone-based colorimetry across most of the color spectrum, with particular efficacy for chromatic colors in the mid-range of brightness. Additional testing under varied lighting conditions (available in supporting information) confirms that these improvements are consistently achieved across different illumination scenarios.

3.4 Application of Color Correction to Video Analysis and Reaction Kinetics

Given our team's broader interests in computer vision-enabled reaction monitoring, we concluded our investigation by examining how the same color correction methods could be used to calibrate the colors recorded in frames captured on two different smartphones. To this end, we used the percarbonate-mediated[25] degradation of Blue1 dye (a trityl cation derivative) as a test reaction to explore dynamic color correction in video analysis of chemical reactions. The chosen test reaction builds upon previous educational applications, such as Nalliah's student experiment where Blue1 kinetics were monitored by tracking brightness changes via a light meter cover time.[26] In relation, one of our team's labs has used hydroxylation of crystal violet (another trityl-centred dye) as a means of testing new video recording environments and computer vision software developments.[19]

To understand the Blue1 chromophore, we measured the spectrum for Blue1 across 17 samples (including a blank), spanning five orders of magnitude (Figure 11). From here, we demonstrated kinetics consistent with the expected pseudo-first order decay of Blue1, consistent with related kinetic studies in the literature (Figure 12).[26, 27]

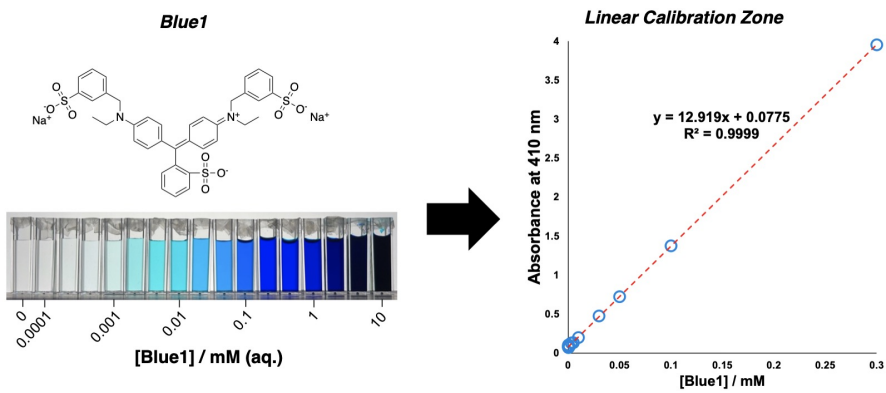


Fig. 11 Left: Chemical structure of Blue1 dye and images of the changing colour of samples over a selected concentration gradient. Right: Linear correlation region used to calibrate absorbance and Blue1 concentration.

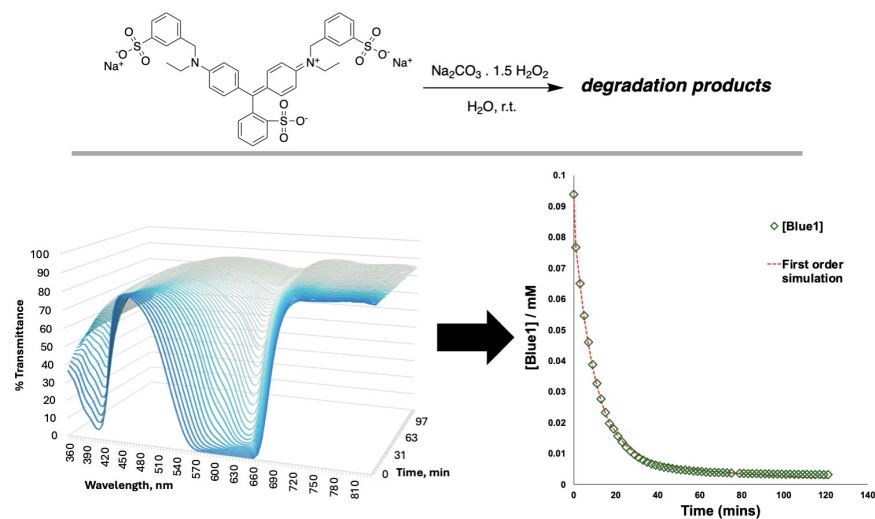


Fig. 12 Spectroscopic approach to kinetic analysis of percarbonate-mediated degradation of Blue1 dye in aqueous solution. $[Blue1]_0 = 0.1 \text{ mM}$, $[\text{Na}_2\text{CO}_3 \cdot 1.5 \text{ H}_2\text{O}_2]_0 = 10 \text{ mM}$, $k_{obs} = 2.8 \times 10^{-6} \text{ s}^{-1}$.

With an established understanding of the reaction kinetics from a traditional spectroscopic perspective, our attention turned to monitoring the reaction with both smartphones, and applying dynamic color correction. For the color analysis of smartphone videos of the Blue1 degradation, we selected the RGB Sum Response as our main color metric, defined as:

$$\text{RGB Sum Response} = 765 - (R + G + B) \quad (11)$$

where 765 is the maximum sum of RGB values ($255 + 255 + 255$) for 8-bit color representation. The lower the RGB Sum Response, the closer the color is to white (765).

Image color correction brings the two smartphones closer to each other. The impact of image color correction on the smartphone video data is shown in Figure 13. Without correction, there is a large disparity between the captured color values of the Blue1 degradation reaction from both cameras. After correction, the color values from both cameras closely follow, as evidenced in a large reduction in the sum of squared differences between the two time series datasets from each smartphone. Overall, the dynamic correction had more impact on the Samsung than on the iPhone data, where color correction compensated for the darker color values captured by the Samsung camera.

SET-UP

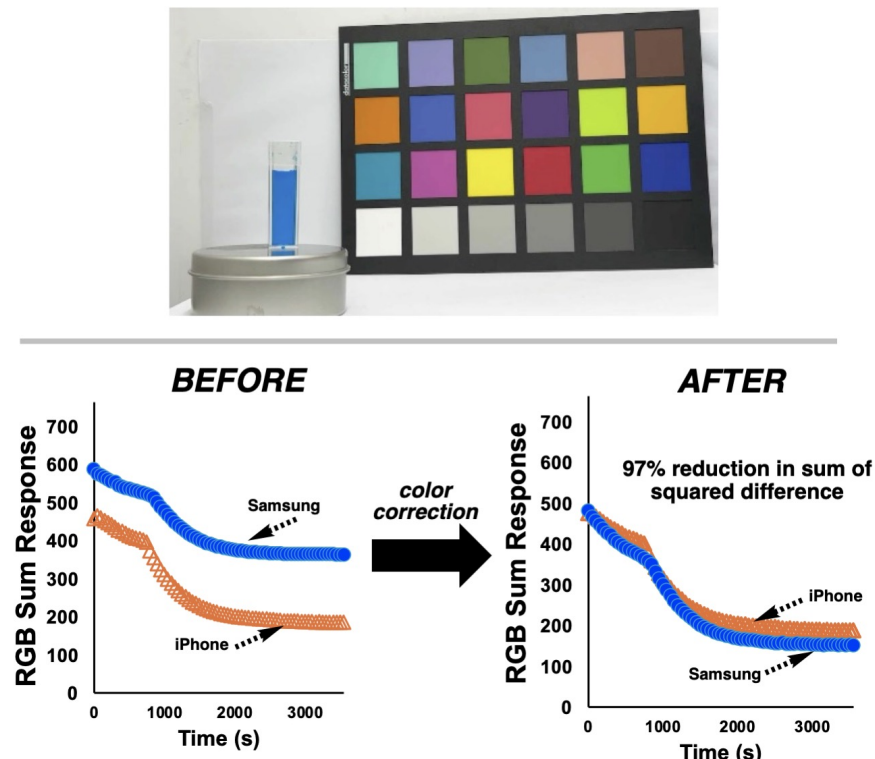


Fig. 13 Top: Set-up used to track Blue1 degradation from each smartphone. The presence of the color checker card in the field of view, present during the entire video recording, enabled dynamic color correction to bring the color data captured on each phone into closer agreement than before correction. Bottom: The impact of dynamic color correction on the level of agreement between smartphones, as captured by RGB Sum Response.

3.5 The impact of Color Gamut Limitations

While we were satisfied at having accomplished our primary goal of demonstrating the possibility of color correction between smartphones for the purpose of reaction monitoring, the investigation of Blue1 degradation by sodium percarbonate serendipitously revealed important distinctions between the kinetic profiles derived from traditional spectrophotometric and smartphone-based digital image colorimetry (DIC) methods. While both techniques quantify color changes, they capture fundamentally different information about the reaction system (Figure 2). Camera sensors capture broad spectral changes across three overlapping color channels rather than monitoring absorbance at discrete wavelengths. Comparing the two dataset sources for monitoring the test reaction, we noticed that profiles of RGB Sum Response versus time, derived from the smartphone camera measurements, contained a 'shouldering' effect approximately 1260 seconds (21 minutes) into the reaction time. No such abrupt change in profile trajectory was observed for the absorbance data derived from the spectrometer (Figure 14).

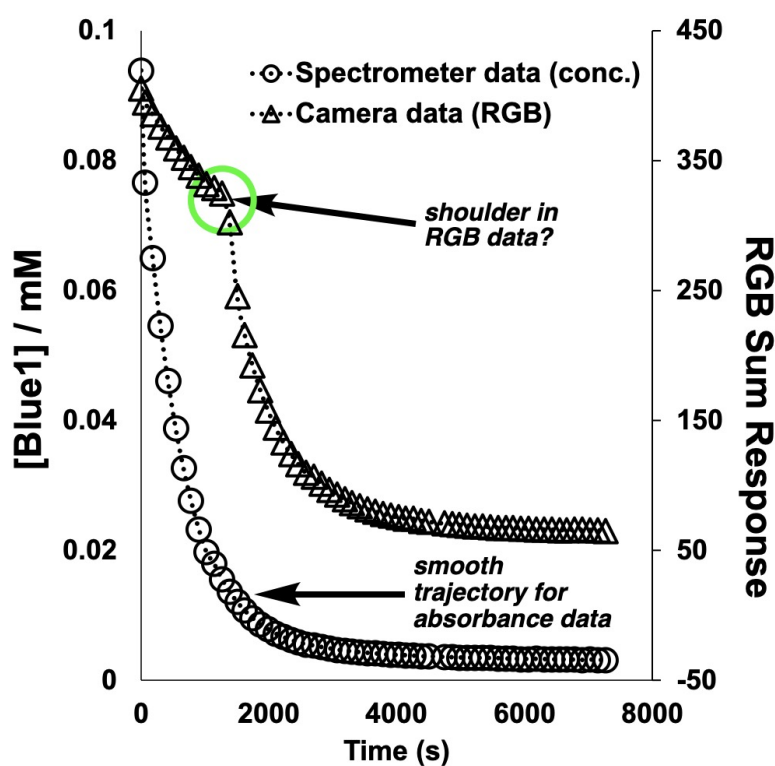


Fig. 14 Highlighting the difference in kinetic trajectories of the time series derived from spectroscopic measurements (open circles) versus smartphone camera measurements (open triangles).

Different measurement paradigms reveal complementary information. Spectrophotometric analysis at specific wavelengths revealed well-behaved pseudo-first-order kinetics for Blue1 degradation, with no apparent shouldering in the absorbance versus time data (Figures 12 and 14). This approach provided a direct relationship between absorbance and concentration at specific wavelengths where the Blue1 trityl cation chromophore absorbs light.

In contrast, the camera-derived RGB-based measurements consistently displayed the characteristic 'shoulder' in the RGB Sum Response profiles. This abrupt shift in the color profile versus time persisted across different lighting conditions and smartphone cameras. Additionally, the effect was not observed in background regions of the same videos. Together, the observations suggested the root cause of the shouldering effect represented a genuine phenomenon specific to the region of interest analysed in the video that captured the evolving reaction mixture. The key question triggered in our minds was therefore: *Is the shouldering effect in the data capturing a chemical phenomenon that only the camera picks up or is it a artifact specific to the camera measurements?*

Color Gamut Limitations in Digital Image Colorimetry

We initially thought the shouldering effect may represent a physical change in the reaction medium (e.g. reaching a threshold change in transparency). However, further analysis of the shouldering effect revealed a fundamental color science phenomenon at its root. During the initial phase of Blue1 degradation, the solution's color exists outside the sRGB color gamut, which is the range of colors that can be represented in standard digital imaging systems. Figure 15 illustrates this phenomenon, showing the trajectory of the reaction in CIE xy chromaticity space.

During approximately the first 21 minutes of reaction, the saturated blue color of the solution produces chromaticity coordinates that lie outside the representable range of the sRGB color space. When converting spectrophotometric data to sRGB or when capturing these colors directly with a smartphone camera, these out-of-gamut colors are 'clipped' (or mapped) to the nearest representable color within the sRGB gamut boundary. This gamut clipping creates an artificial attenuation of the trajectory of sRGB values during the initial reaction phase. When the true color of the reaction mixture finally crosses into the sRGB gamut (approximately at the 21-minute mark), the sRGB values begin to accurately represent the color changes, creating the observed shoulder in the RGB sum response data.

This phenomenon affects both spectra-derived RGB values and direct camera measurements, though cameras may implement different gamut mapping algorithms that affect exactly how out-of-gamut colors are represented. The shoulder therefore represents a fundamental limitation of RGB-based colorimetry when monitoring reactions involving saturated colors that exceed the gamut limitations of standard digital color spaces.

This gamut limitation effect represents an important consideration for the digital image colorimetry field that has not been thoroughly documented in previous literature, particularly in the context of reaction monitoring where color trajectories may cross gamut boundaries during the course of the reaction. For reactions involving

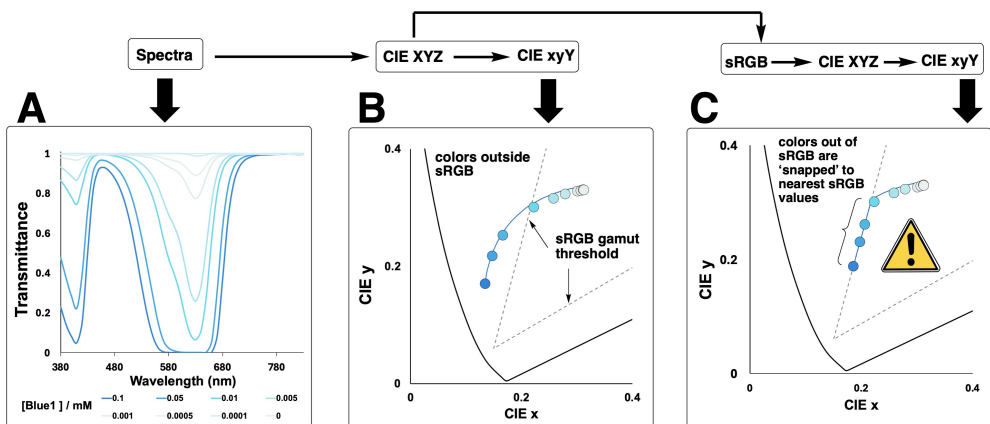


Fig. 15 Demonstrating how the operative sRGB color gamut subset of the xy chromaticity diagram artificially limits the range of colors mapped during the Blue1 degradation reaction. **A** → **B**: Converting spectral data to the xyY color space shows faithful mapping of the Blue1 degradation, inside and outside the threshold of sRGB gamut region. **B** → **C**: Converting the xyY colors to sRGB and then back to xyY shows an artificial 'clipping' of the colors at time points up to the first 21 minutes of the Blue1 degradation reaction, coincident with the time of the observed shouldering effect shown in Figure 14. Thereafter, the colors in the latter stage of the degradation reaction are mapped faithfully.

highly saturated colors, the apparent kinetics derived from RGB camera data may not accurately reflect the true reaction profile during periods when the colors exceed the representable gamut. Alternative color spaces with wider gamuts (such as Adobe RGB or ProPhoto RGB) may partially mitigate this issue, but ultimately, spectrophotometric measurements remain necessary for accurately quantifying the concentration of intensely colored species that fall outside standard RGB gamuts. That said, the value of non-contact video-based monitoring of chemical reactions remains its privileged place in capturing the reaction bulk, complementary to more common efforts to capture molecular specifics.^[18]

4 Conclusion

The value of image color correction for digital colorimetry extends far beyond laboratory settings, offering a strategy to enhance reproducibility in analytical workflows across diverse environments. Our comprehensive investigation has revealed several key insights:

- While sensor variability between smartphone models contributes minimally to measurement discrepancies ($\Delta E < 0.5$), environmental factors, particularly lighting conditions and capture angles, significantly impact color accuracy, with ΔE values increasing by up to 64% at oblique viewing angles.
- Our matrix-based color correction approach successfully reduced inter-device and lighting-dependent variations by 65-70%, bringing smartphone-derived measurements into closer alignment with reference spectrophotometric data.

- When applied to time-resolved video analysis of Blue1 dye degradation by sodium percarbonate, the color correction methodology enabled consistent kinetic profiles across different smartphone models, comparable to those obtained via traditional spectrophotometry.
- We identified an important limitation in RGB-based colorimetry: the sRGB color gamut boundary creates artificial discontinuities in reaction monitoring when highly saturated colors exceed the representable range, manifesting as 'shouldering' effects in kinetic profiles.

This work bridges the divide between conventional laboratory instrumentation and mobile analytical chemistry, establishing a framework for more accessible and reproducible color-based measurements. In settings where standardized instrumentation is limited, including field diagnostics, industrial production lines, or decentralized quality control, the combination of ubiquitous smartphone hardware and reference color charts offers a scalable, cost-effective solution for consistent color-based analytics.

Future research should focus on advancing this methodology through: (1) development of more sophisticated non-linear correction algorithms that better account for the complex relationships between camera sensors and ambient lighting; (2) implementation of automated color chart detection and region-of-interest selection to streamline the correction process; (3) integration of machine learning approaches to compensate for color gamut limitations; and (4) exploration of wider-gamut color spaces to more accurately represent highly saturated chromophores.

By enhancing the robustness of digital image colorimetry across different devices and environments, our color correction methodology facilitates standardized measurements even under variable conditions, enabling broader application of smartphone-based and time-resolved colorimetric techniques in fields ranging from environmental monitoring to point-of-care diagnostics.

Acknowledgments

CF and MR thanks Singapore's Agency for Science, Technology and Research (A*STAR) for PhD funding support through A*STAR Research Attachment Programme (ARAP). Any opinions, findings and conclusions or recommendations expressed in this material are those of the author(s) and do not reflect the views of A*STAR. MR thanks the UK Research & Innovation for Future Leaders Fellowship funding (MR/T043458/1).

Declarations

M.R. is the inventor of Kineticolor and leading the software commercialization process. For information on licensing Kineticolor software, please contact the corresponding author and the University of Strathclyde technology transfer office:

marc.reid.100@strath.ac.uk; iprmanager@strath.ac.uk

Data Availability Statement

A zipped folder of machine-readable data, ordered according to the Figure numbers in the main text, is available on figshare at: <https://doi.org/10.6084/m9.figshare.28996382.v1>

References

- [1] da Nobrega Gaiao, E. *et al.* Digital image-based titrations. *Analytica Chimica Acta* **570**, 283–290 (2006). URL <https://www.sciencedirect.com/science/article/pii/S0003267006008634>.
- [2] Capitán-Vallvey, L. F., López-Ruiz, N., Martínez-Olmos, A., Erenas, M. M. & Palma, A. J. Recent developments in computer vision-based analytical chemistry: A tutorial review. *Analytica Chimica Acta* **899**, 23–56 (2015). URL <https://www.sciencedirect.com/science/article/pii/S000326701501243X>.
- [3] Fan, Y., Li, J., Guo, Y., Xie, L. & Zhang, G. Digital image colorimetry on smartphone for chemical analysis: A review. *Measurement* **171**, 108829 (2021). URL <https://www.sciencedirect.com/science/article/pii/S0263224120313221>.
- [4] Markus, V., Paul, A. A., Marks, R. S. & and, J. C. Smartphone digital image colorimetry: An affordable easy-to-use technique. *Analytical Letters* **0**, 1–19 (2025). URL <https://doi.org/10.1080/00032719.2025.2474573>.
- [5] Hou, P. *et al.* A wifi scanner in conjunction with disposable multiplex paper assay for the quantitation of disease markers in blood plasma. *Analytical and Bioanalytical Chemistry* **413**, 4625–4634 (2021). URL <https://doi.org/10.1007/s00216-021-03234-6>.
- [6] Akhoundian, M., Khaki, M. & Alizadeh, T. Ultra-selective colorimetric sensor based on molecularly imprinted polymer for proline detection in food samples. *Spectrochimica Acta Part A: Molecular and Biomolecular Spectroscopy* **332**, 125860 (2025). URL <https://www.sciencedirect.com/science/article/pii/S1386142525001660>.
- [7] Garmay, A. V., Oskolok, K. V., Monogarova, O. V. & Demidov, M. I. Determination of ammonium and nitrate in soils by digital colorimetry. *Environmental Monitoring and Assessment* **196**, 948 (2024). URL <https://doi.org/10.1007/s10661-024-13068-1>.
- [8] Barbosa, L. S. V., Strauch, P., Santos, D. C. M. B., Korn, M. & Santana, R. M. M. Homemade paper analytical device and digital image colorimetry as tools for learning about calibration curve methods during the covid pandemic: A remote vs in-person class evaluation. *Journal of Chemical Education* **100**, 2601–2607 (2023). URL <https://doi.org/10.1021/acs.jchemed.2c01081>. Doi: 10.1021/acs.jchemed.2c01081.

- [9] Zeng, X. *et al.* Cloud machine learning-enhanced peroxidase-like enzyme visual sensor for rapid detection of sulfur-containing pesticides. *Sensors and Actuators B: Chemical* **431**, 137448 (2025). URL <https://www.sciencedirect.com/science/article/pii/S0925400525002230>.
- [10] Ichsan, C., Ramadhan, N., Arsana, K. G. Y., Syamsuri, M. M. F. & Rohmatul-laili. Enhanced co₂ leak detection in soil: High-fidelity digital colorimetry with machine learning and aces ap0. *Chemometrics and Intelligent Laboratory Systems* **255**, 105268 (2024). URL <https://www.sciencedirect.com/science/article/pii/S0169743924002089>.
- [11] Ichsan, C. & Rodiah, S. The best performing color space and machine learning regression algorithm for the accurate estimation of chromium (vi) and iron (iii) in aqueous samples using low-cost and portable flatbed scanner colorimetry. *Journal of the Iranian Chemical Society* **21**, 2335–2349 (2024). URL <https://doi.org/10.1007/s13738-024-03073-z>.
- [12] Canovas-Saura, A., Serrano-Lujan, L., Beltran, V. & Padilla, J. Neural network-based digital camera spectrophotometer: Application to chromogenic technologies characterization. *ACS Applied Optical Materials* **2**, 1403–1412 (2024). URL <https://doi.org/10.1021/acsaom.4c00180>. Doi: 10.1021/acsaom.4c00180.
- [13] Tominaga, S., Nishi, S. & Ohtera, R. Measurement and estimation of spectral sensitivity functions for mobile phone cameras. *Sensors* **21**, 21 (2021). URL <https://doi.org/10.3390/s21154985>.
- [14] da Penha, G. M., Pereira, A. V., Tavares, E., dos Santos, D. & Fatibello-Filho, O. Microplate-based 3d-printed image box for urea determination in milk by digital image colorimetry. *Anal. Methods* **16**, 5676–5683 (2024). URL <http://dx.doi.org/10.1039/D4AY01191K>.
- [15] Li, W., Liu, F., He, Y. & Song, G. A ratiometric fluorescent sensor based on s-doped bcno quantum dots and au nanoclusters combined with 3d-printing portable device for the detection of malachite green. *Microchimica Acta* **191** (2024). URL <https://doi.org/10.1007/s00604-024-06465-3>.
- [16] Mirhosseini, S. *et al.* A digital image colorimetry system based on smart devices for immediate and simultaneous determination of enzyme-linked immunosorbent assays. *Scientific Reports* **14**, 2587 (2024). URL <https://doi.org/10.1038/s41598-024-52931-6>.
- [17] Meng, R. *et al.* Smartphone-based colorimetric detection platform using color correction algorithms to reduce external interference. *Spectrochimica Acta Part A: Molecular and Biomolecular Spectroscopy* **316**, 124350 (2024). URL <https://www.sciencedirect.com/science/article/pii/S138614252400516X>.

- [18] Fyfe, C., Barrington, H., Gordon, C. M. & Reid, M. A computer vision approach toward verifying cfd models of stirred tank reactors. *Organic Process Research & Development* **28**, 3661–3673 (2024). URL <https://doi.org/10.1021/acs.oprd.4c00229>. Doi: 10.1021/acs.oprd.4c00229.
- [19] Barrington, H. *et al.* Parallel and high throughput reaction monitoring with computer vision. *Angewandte Chemie-International Edition* **64**, 10 (2025). URL <https://doi.org/10.1002/anie.202413395>.
- [20] Bugeja, N. *et al.* Teaching old presumptive tests new digital tricks with computer vision for forensic applications. *Digital Discovery* **2**, 1143–1151 (2023). URL <https://doi.org/10.1039/D3DD00066D>.
- [21] Chang, H. Y. *et al.* Presumptive tests for xylazine-a computer vision approach. *Anal. Sci. Adv.* **6**, e70008 (2025).
- [22] Yan, C. *et al.* Computer vision for non-contact monitoring of catalyst degradation and product formation kinetics. *Chemical Science* **14**, 5323–5331 (2023).
- [23] Li, C. *et al.* Accurate method for computing correlated color temperature. *Optics Express* **24**, 14066–14078 (2016). URL <https://opg.optica.org/oe/abstract.cfm?URI=oe-24-13-14066>.
- [24] MacAdam, D. L. Visual sensitivities to color differences in daylight*. *Journal of the Optical Society of America* **32**, 247–274 (1942). URL <https://opg.optica.org/abstract.cfm?URI=josa-32-5-247>.
- [25] Sukhatskiy, Y. & Lysak, D. in *Chapter 15 - sodium percarbonate-based advanced oxidation processes* (ed.Hamdaoui, O.) *Innovative and Hybrid Advanced Oxidation Processes for Water Treatment* 389–406 (Elsevier, 2025). URL <https://www.sciencedirect.com/science/article/pii/B9780443141003000090>.
- [26] Nalliah, R. E. Reaction of fd&c blue 1 with sodium percarbonate: Multiple kinetics methods using an inexpensive light meter. *Journal of Chemical Education* **96**, 1453–1457 (2019). URL <https://doi.org/10.1021/acs.jchemed.8b00589>. Doi: 10.1021/acs.jchemed.8b00589.
- [27] Thompson, K. M., Griffith, W. P. & Spiro, M. Mechanism of bleaching by peroxides. part 1.—kinetics of bleaching of phenolphthalein by hydrogen peroxide at high ph. *J. Chem. Soc., Faraday Trans.* **89**, 1203–1209 (1993). URL <http://dx.doi.org/10.1039/FT9938901203>.